



**HAL**  
open science

## Blood flow diverts extracellular vesicles from endothelial degradative compartments to promote angiogenesis

Benjamin Mary, Nandini Asokan, Katerina Jerabkova-roda, Annabel Larnicol, Ignacio Busnelli, Tristan Stemmelen, Raphaël Carapito, Olivier Lefebvre, Jacky G Goetz, Vincent Hyenne

### ► To cite this version:

Benjamin Mary, Nandini Asokan, Katerina Jerabkova-roda, Annabel Larnicol, Ignacio Busnelli, et al.. Blood flow diverts extracellular vesicles from endothelial degradative compartments to promote angiogenesis. *EMBO Reports*, 2023, 10.15252/embr.202357042 . hal-04297597

**HAL Id: hal-04297597**

**<https://hal.science/hal-04297597>**









Submitted on 21 Nov 2023

**HAL** is a multi-disciplinary open access archive for the deposit and dissemination of scientific research documents, whether they are published or not. The documents may come from teaching and research institutions in France or abroad, or from public or private research centers.

L'archive ouverte pluridisciplinaire **HAL**, est destinée au dépôt et à la diffusion de documents scientifiques de niveau recherche, publiés ou non, émanant des établissements d'enseignement et de recherche français ou étrangers, des laboratoires publics ou privés.

SOURCE  
DATATRANSPARENT  
PROCESSOPEN  
ACCESS

# Blood flow diverts extracellular vesicles from endothelial degradative compartments to promote angiogenesis

Benjamin Mary<sup>1,2,3,4,†</sup> , Nandini Asokan<sup>1,2,3,4,†</sup> , Katerina Jerabkova-Roda<sup>1,2,3,4</sup> , Annabel Larnicol<sup>1,2,3,4</sup>,  
Ignacio Busnelli<sup>1,2,3,4</sup>, Tristan Stemmelen<sup>1,2,3,5,6</sup> , Angélique Pichot<sup>1,2,3,5</sup> , Anne Molitor<sup>1,2,3,5</sup> ,  
Raphaël Carapito<sup>1,2,3,5,6</sup> , Olivier Lefebvre<sup>1,2,3,4</sup> , Jacky G Goetz<sup>1,2,3,4,\*,‡</sup>  & Vincent Hyenne<sup>1,2,3,4,7,\*\*,‡</sup> 

## Abstract

Extracellular vesicles released by tumors (tEVs) disseminate via circulatory networks and promote microenvironmental changes in distant organs favoring metastatic seeding. Despite their abundance in the bloodstream, how hemodynamics affect the function of circulating tEVs remains unsolved. We demonstrated that efficient uptake of tEVs occurs in venous endothelial cells that are subjected to hemodynamics. Low flow regimes observed in veins partially reroute internalized tEVs toward non-acidic and non-degradative Rab14-positive endosomes, at the expense of lysosomes, suggesting that endothelial mechanosensing diverts tEVs from degradation. Subsequently, tEVs promote the expression of pro-angiogenic transcription factors in low flow-stimulated endothelial cells and favor vessel sprouting in zebrafish. Altogether, we demonstrate that low flow regimes potentiate the pro-tumoral function of circulating tEVs by promoting their uptake and rerouting their trafficking. We propose that tEVs contribute to pre-metastatic niche formation by exploiting endothelial mechanosensing in specific vascular regions with permissive hemodynamics.

**Keywords** angiogenesis; extracellular vesicles; hemodynamics; lysosomal degradation; metastasis

**Subject Categories** Cancer; Membranes & Trafficking; Vascular Biology & Angiogenesis

**DOI** 10.15252/embr.202357042 | Received 20 February 2023 |

Revised 19 October 2023 | Accepted 27 October 2023

**EMBO Reports (2023) e57042**

## Introduction

Inter-organ communication is instrumental in maintaining systemic homeostasis, in coordinating metabolic response to environmental challenges or in reacting to diseased tissue. It can be mediated by hormones, cytokines, but also by membrane-covered structures belonging to the heterogeneous family of extracellular vesicles (EVs) (Tkach & Théry, 2016). These small vesicles (30 nm to 5 µm diameter range) transport bioactive molecules (RNAs, lipids, proteins) between distant organs by traveling through circulatory networks (Yáñez-Mó *et al*, 2015; Cheng & Hill, 2022). In cancer, as the disease becomes systemic and progresses from primary to secondary sites, EVs actively contribute to organ cross-talk and thereby impact both primary tumor growth and metastatic spreading. Tumor EVs (tEVs) released by primary tumors spread via blood or lymphatic circulation and reach distant organs where they alter the microenvironment (Kalluri & LeBleu, 2020; Marar *et al*, 2021). When reaching future metastatic organs before tumor cells arrival, tEVs modify their cellular and extracellular composition and create a pre-metastatic niche favorable to metastasis formation (Peinado *et al*, 2017; Ghoroghi *et al*, 2021a). While the changes induced by tEVs on distant organs started to be unraveled over the past years, the transit of tEVs from the circulation to the new organ are very poorly described. Notably, while circulating tEVs are mostly taken up by endothelial cells (together with intravascular patrolling monocytes) in both vascular blood (Takahashi *et al*, 2013; Imai *et al*, 2015; Morishita *et al*, 2015; Hyenne *et al*, 2019) and lymphatic settings (García-Silva *et al*, 2021), few studies described

1 INSERM UMR\_S1109, Strasbourg, France

2 Université de Strasbourg, Strasbourg, France

3 Fédération de Médecine Translationnelle de Strasbourg (FMTS), Strasbourg, France

4 Équipe Labellisée Ligue Contre le Cancer, Strasbourg, France

5 Plateforme GENOMAX, Institut thématique interdisciplinaire (ITI) de Médecine de Précision de Strasbourg Transplantex NG, Fédération Hospitalo-Universitaire OMICARE, Strasbourg, France

6 Service d'Immunologie Biologique, Hôpitaux Universitaires de Strasbourg, Strasbourg, France

7 CNRS, SNC5055, Strasbourg, France

\*Corresponding author. Tel: +33 388853847; E-mail: [jacky.goetz@inserm.fr](mailto:jacky.goetz@inserm.fr)

\*\*Corresponding author. Tel: +33 388853323; E-mail: [hyenne@unistra.fr](mailto:hyenne@unistra.fr)

†These authors contributed equally to this work

‡These authors contributed equally to this work

their fate in a realistic vascular environment (Hyenne *et al*, 2019; Verweij *et al*, 2019b; van Niel *et al*, 2022). By contrast, the behavior of circulating tumor cells (CTCs) in the vasculature is better understood (Follain *et al*, 2020). For instance, it is now well established that blood flow forces (i.e. flow velocity and shear stress) directly impact the arrest, extravasation and metastatic capacities of circulating tumor cells (Follain *et al*, 2020). We thus hypothesized that hemodynamics is likely to tune the vascular targeting and uptake of tEVs and thereby control how they prime distant organs and form pre-metastatic niches.

Furthermore, hemodynamics strongly affects the biology of the endothelium: through a variety of mechano-sensors, endothelial cells sense and rapidly respond to flow forces, notably to shear stress, by adapting their architecture and homeostasis (Fang *et al*, 2019). For instance, hemodynamic forces alter endothelial shape and cytoskeleton organization (Li *et al*, 2005), but also endosomal pathways, such as endothelial autophagy (Vion *et al*, 2017). Flow shear forces also directly impact the capacity of endothelial cells to take up material flowing in the circulation, such as ions, proteins, or nanoparticles, although it is not clear whether they alter their fate (Tarbell, 2010; Han *et al*, 2012, 2015). Therefore, we speculated that hemodynamics would impact the fate and trafficking of internalized tEVs.

To test this possibility, we built an experimental pipeline that allows to control flow forces while assessing the initial steps of tEVs targeting, uptake and fate in realistic hemodynamic environments. We chose to use EVs isolated from a triple-negative breast cancer line, 4T1, as we have shown that they prime pre-metastatic niches in secondary organs (Ghoroghi *et al*, 2021b). Here, we combined an *in vivo* model, the zebrafish embryo, that we adapted to the study of tEVs (Hyenne *et al*, 2019; Verweij *et al*, 2019a), together with an *in vitro* microfluidics models where a monolayer of endothelial cells can be challenged with tunable flow profiles (Follain *et al*, 2018). Such multi-modal approach allowed to document, for the first time, how hemodynamics control the trafficking of tEVs upon uptake, whose consequences are instrumental in mediating their microenvironmental priming function. We show that specific venous hemodynamics where high tEVs uptake occurs, regulates their fate and function through the control of their trafficking routes in endothelial cells. Importantly, we show that low flow regimes promote a partial

lysosomal escape which enhances the pro-angiogenic function of tEVs.

## Results

### Blood flow tunes endothelial uptake of circulating tEVs

To determine the influence of hemodynamics on the dissemination of circulating tEVs, we took advantage of the zebrafish embryo (Hyenne *et al*, 2019). At 48 h post-fertilization, the zebrafish embryo is composed of a complex vascular network suited to real-time imaging of circulating EVs (Hyenne *et al*, 2019; Verweij *et al*, 2019a, 2021). When injected in the Duct of Cuvier, tEVs quickly disseminate through the bloodstream and reach the caudal plexus via the dorsal aorta (Fig 1A and Hyenne *et al*, 2019). While the dorsal aorta carries circulating tEVs at flow velocities exceeding 550  $\mu\text{m/s}$ , these quickly return in venous compartments characterized by low flow velocities (Average < 450  $\mu\text{m/s}$ ) (Follain *et al*, 2018). Interestingly, when assessing which vascular regions were preferably targeted by tEVs, we observed that both patrolling macrophages and endothelial cells of low flow regions efficiently internalized circulating tEVs (Hyenne *et al*, 2019). We first validated tEVs uptake by endothelial cells by correlating intravital imaging with electron microscopy (iCLEM) (Fig 1A, iCLEM panel, Fig EV1). We then carefully and concomitantly measured blood flow velocities and endothelial accumulation of circulating tEVs (Fig 1A). To do so, we isolated tEVs from tumor cells by differential centrifugation, labeled them with MemGlow (Collot *et al*, 2018; Hyenne *et al*, 2019) and injected them in the circulation of zebrafish embryos (Mary *et al*, 2020). We analyzed four vascular regions (Fig 1A, hemodynamics panel) that are representatives of the flow profiles found in the caudal plexus and plotted the amount of tEVs internalized by endothelial cells with respect to the flow velocities (Fig 1A and Movie EV1). We observed that the data segregated in two populations with respect to endothelial cell position: while accumulation of tEVs is maximal in regions of the caudal vein averaging 400–450  $\mu\text{m/s}$  flow velocity, it is significantly reduced in regions of the dorsal aorta where flow ranges from 575 to 650  $\mu\text{m/s}$ . Of note, we observed a similar pattern using 4T1 EVs isolated by

**Figure 1. Blood flow tunes the uptake of circulating tEVs by endothelial cells.**

- A Description of the experimental setup: 2 days post-fertilization (Flil:GFP (endothelium) Gata1:dsRed (red blood cells; RBCs) zebrafish embryos are injected intravascularly (i.v.) via the duct of Cuvier with Memglow-Cy5-labeled 4T1 tEVs and imaged in the caudal plexus after 30 min (right, Z projection). iCLEM panel: EVs injected embryos were imaged live, fixed and processed for CLEM. Endothelial regions were EVs were observed by photon microscopy are retrieved by electron microscopy (red arrows) and contain endosomal structures. Hemodynamics panel: Velocities of individual circulating RBCs are tracked and fluorescent tEV signal internalized in the endothelium is measured in four indicated regions per fish (2 dorsal aorta and 2 caudal vein). Bottom left: representative images of the four regions showing tEVs within the endothelium (Z projections) and RBCs tracks with a color code representing velocities (white arrows indicate the direction of the flow). Bottom right: graph showing the correlation between internalized tEVs and RBC velocities in the four different regions ( $n = 6$  embryos, three independent experiments).
- B, C Memglow-Cy5-labeled 4T1 tEVs are injected intravascularly (i.v.) in Flil:GFP (GFP endothelium) embryos with decreased (B) or increased (C) heart pacemaker activity with respectively lidocaine and IBMX treatments. Middle: representative images, maximum intensity projections. Yellow stars: patrolling macrophages. Right graph represents the percentage of fluorescent tEVs within the endothelium (1 dot: 1 fish; Lidocain:  $n = 36$  per condition, three independent experiments; \*\*\*\* $P < 0.0001$  Student *t*-test; IBMX:  $n = 39$  per condition, three independent experiments,  $P = 0.11$  Student *t*-test; n.s., non significant).
- D Memglow-Cy5-labeled 4T1 tEVs are perfused on HUVECs endothelial monolayer labeled with Memglow 488 in static or flow conditions (400  $\mu\text{m/s}$ , corresponding to a 0.43  $\text{dyn/cm}^2$  shear stress) and imaged by confocal microscope after 3 h. Representative images and quantification of internalized tEVs showing increase in tEV total fluorescence ( $P = 0.013$ , Mann–Whitney) and in tEV total area ( $P = 0.0001$ , Mann–Whitney) (data per cell, normalized to static; 1 dot: 1 field of view;  $n = 67$ ; experiment performed in quintuplicate). (a.u. arbitrary units). \* $P < 0.05$ ; \*\*\*\* $P < 0.001$ .

Source data are available online for this figure.

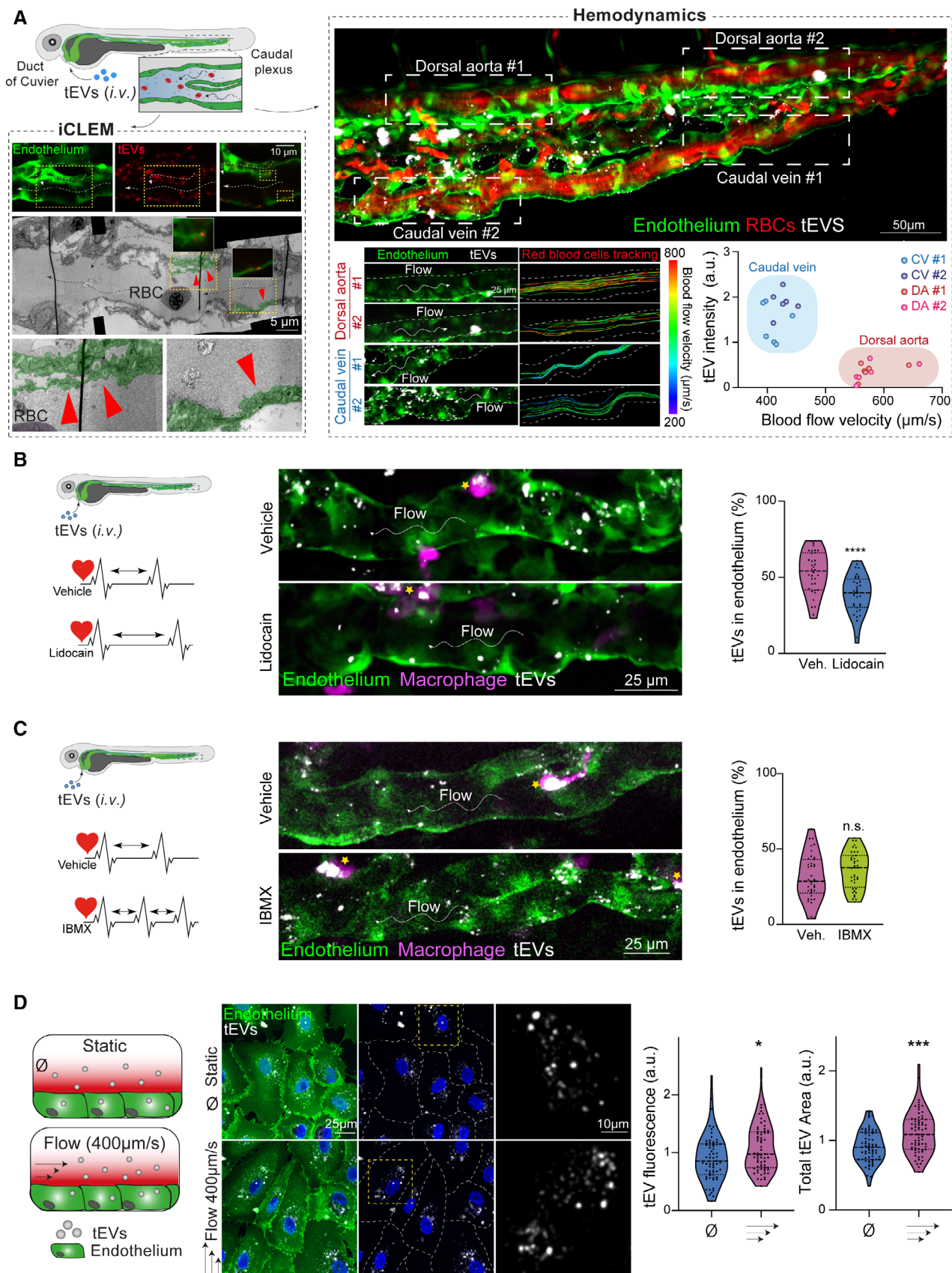


Figure 1.

size exclusion chromatography and with EVs from AT3 cells, another triple-negative breast cancer cell line (Fig EV2A and B). In order to explore whether flow profiles directly impact the uptake of tEVs, we pharmacologically tuned blood flow velocities in the zebrafish embryo and quantified the resulting tEVs uptake in the caudal vein. Decreasing flow velocities with lidocaine (Fig EV2C), a sodium channel blocker that reduces pacemaker activity of the heart (Follain *et al*, 2018), lead to a significant decrease of tEVs uptake by endothelial cells of the caudal vein (Fig 1B). Conversely, increasing the heart pacemaker activity (Fig EV2C) using IBMX (3-isobutyl-1-methylxanthine) (Follain *et al*, 2018) results in a slight albeit non-significant increase in tEVs uptake (Fig 1C). These data suggest that tEVs uptake is optimal in endothelial cells of the caudal vein that is subjected to lower flow regimes averaging 400  $\mu\text{m/s}$ . Notably, a careful analysis of the correlation between EV internalization, vascular regions and their associated blood flow profiles reveals that venous endothelial cells always showed superior EV uptake levels when flow is pharmacologically manipulated (Fig EV2C). This suggests that the EV uptake potential of endothelial cells of the caudal vein exceeds the one of the dorsal aorta and implies that, in addition to hemodynamics, the identity of endothelial cells contributes to EV uptake. While this question would require further investigation, we decided to focus the rest of our study on venous endothelial cells, as they internalize most of circulating EVs. To confirm these *in vivo* data suggesting that tEVs uptake is mostly efficient at velocity flow profiles averaging 400  $\mu\text{m/s}$  occurring in venous regions, we exploited an *in vitro* microfluidics system, which allows for a precise and homogenous control of flow regimes on a monolayer of endothelial cells of venous identity (HUVECs, Fig 1D, left). Similarly, we measured the internalization of fluorescent tEVs perfused and observed that tEVs accumulate more efficiently in endothelial cells subjected to a 400  $\mu\text{m/s}$  flow speed (which we estimate to correspond to shear stress value of 0.43  $\text{dyn/cm}^2$ ) when compared to static (or no flow) conditions (Fig 1D, right). Similar results were obtained using genetically labeled CD63-APEX2-GFP EVs (Fig EV2D). Interestingly, at higher flow speed (4,400  $\mu\text{m/s}$  corresponding to an estimated shear stress value of 5  $\text{dyn/cm}^2$ ), the total

amount of internalized EVs remains similar, yet with heterogeneous distribution among endothelial cells (Fig EV2D). Altogether, our *in vitro* and *in vivo* experiments demonstrate that efficient uptake of tEVs occurs in venous endothelial cells where low blood flow has a positive effect on EV internalizations.

### Circulating tEVs are partially re-routed to alternative non-acidic and non-degradative RAB14 positive compartments

We then aimed to characterize the fate of circulating tEVs in low flow-stimulated endothelial cells. To investigate the trafficking routes exploited by tEVs, we generated vHUVECs endothelial cell lines stably expressing fluorescent markers of early (mCherry-Rab5), late (mEmerald-Rab7) and recycling endosomes (eGFP-Rab11) as well as late endosome-lysosomes (RFP-LAMP1). We tracked the internalization of fluorescently labeled tEVs by live imaging and quantified their colocalization with endosomal markers after 3 h using an automated image analysis pipeline (see Materials and Methods). We found that internalized tEVs mostly co-localize with LAMP1 and, to a lesser extent with Rab5 and Rab7 positive compartments (Figs 2A and EV3A–C). A low flow regime had no effect on the distribution of tEVs among these endosomal markers suggesting that endothelial mechanosensing had no impact on the general internalization routes used by tEVs.

The accumulation of circulating tEVs in LAMP1 positive compartments suggests that they could mostly be stored in degradative compartments, similarly to what happens in patrolling macrophages (Hyenne *et al*, 2019). Therefore, we interrogated whether flow could divert tEVs from degradative machineries. We first labeled degradative compartments in endothelial cells using the Magic Red membrane permeant probe, which detects the activity of the lysosomal protease cathepsin B. While most of the internalized tEVs accumulate in Magic Red positive compartments, flow significantly reduced the proportion of tEVs found in cathepsin B-positive structures (Fig 2B) suggesting that internalized tEVs are partially redirected to non-degradative compartments upon flow mechanosensing. Since the degradative activity of lysosomes hydrolases relies on the acidic

#### Figure 2. Blood flow diverts tEVs sorting toward RAB14 positive non-degradative and non-acidic compartments.

- A *In vitro*, internalized tEVs co-localize more efficiently with LAMP1 than RAB5, RAB7 and RAB11 in endothelial cells cultured under flow. Memglo-Cy5 labeled tEVs were perfused on vHUVECs cells stably expressing FP-RAB5,7,11 or LAMP1 cultured in flow or static conditions and imaged by spinning disk after 3 h (single plane representative images). Automated colocalization analysis (Mann–Whitney, n.s.:non significant, one dot = one cell,  $n = 7–20$  from two to three independent experiments).
- B Decreased accumulation of circulating tEVs in degradative compartments in endothelial cells cultured under flow. Memglo-Cy5 labeled tEVs were perfused on HUVECs cultured in flow or static conditions and labeled using Magic Red to stain compartments with cathepsin B activity. Representative spinning disk single plane images (Manual quantification, one dot = one cell,  $n = 30$  from three independent experiments, Mann–Whitney, \*\*\*\* $P < 0.0001$ ).
- C tEVs accumulate in less acidic compartments when endothelial cells are cultured under flow. CD63-pHluorin-mScarlet 4T1 EVs were perfused on HUVECs cultured in flow or static condition and imaged by spinning disk after 3 h (single plane representative images). Graph represents the pHluorin/mScarlet ratio (one dot = one field of view,  $n = 15$ , experiment performed in triplicate Mann–Whitney, \*\*\*\* $P < 0.0001$ ).
- D tEVs show increased accumulation in Rab14 positive compartments in endothelial cells cultured under flow. Memglo-Cy5 labeled tEVs were perfused on vHUVECs cells stably expressing GFP-RAB14 cultured in flow or static conditions and imaged by spinning disk after 3 h (single plane representative images). Manual and automated quantifications show increased colocalization in flow conditions (one dot = one cell,  $n > 139$  from four independent experiments, Mann–Whitney, \*\*\*\* $P < 0.0001$ ).
- E In zebrafish embryos, modulating flow speed alters tEVs trafficking in acidic compartments. CD63-pHluorin-mScarlet 4T1 tEVs were injected intravascularly (i.v.) in wild-type zebrafish embryos treated with lidocaine or IBMX to respectively decrease or increase heartbeat rates and flow velocity (veh., vehicle). Maximum projection of fish caudal vein area showing tEVs accumulation in the endothelium (visualized by transmitted light and represented with a white dashed line) 3 h post-injection. Graph represents the pHluorin/mScarlet ratio in venous endothelial cells (one dot = one fish (average of individual single Z plans),  $n > 22$  embryos from three independent experiments, Mann–Whitney, \* $P < 0.05$ ).

Source data are available online for this figure.

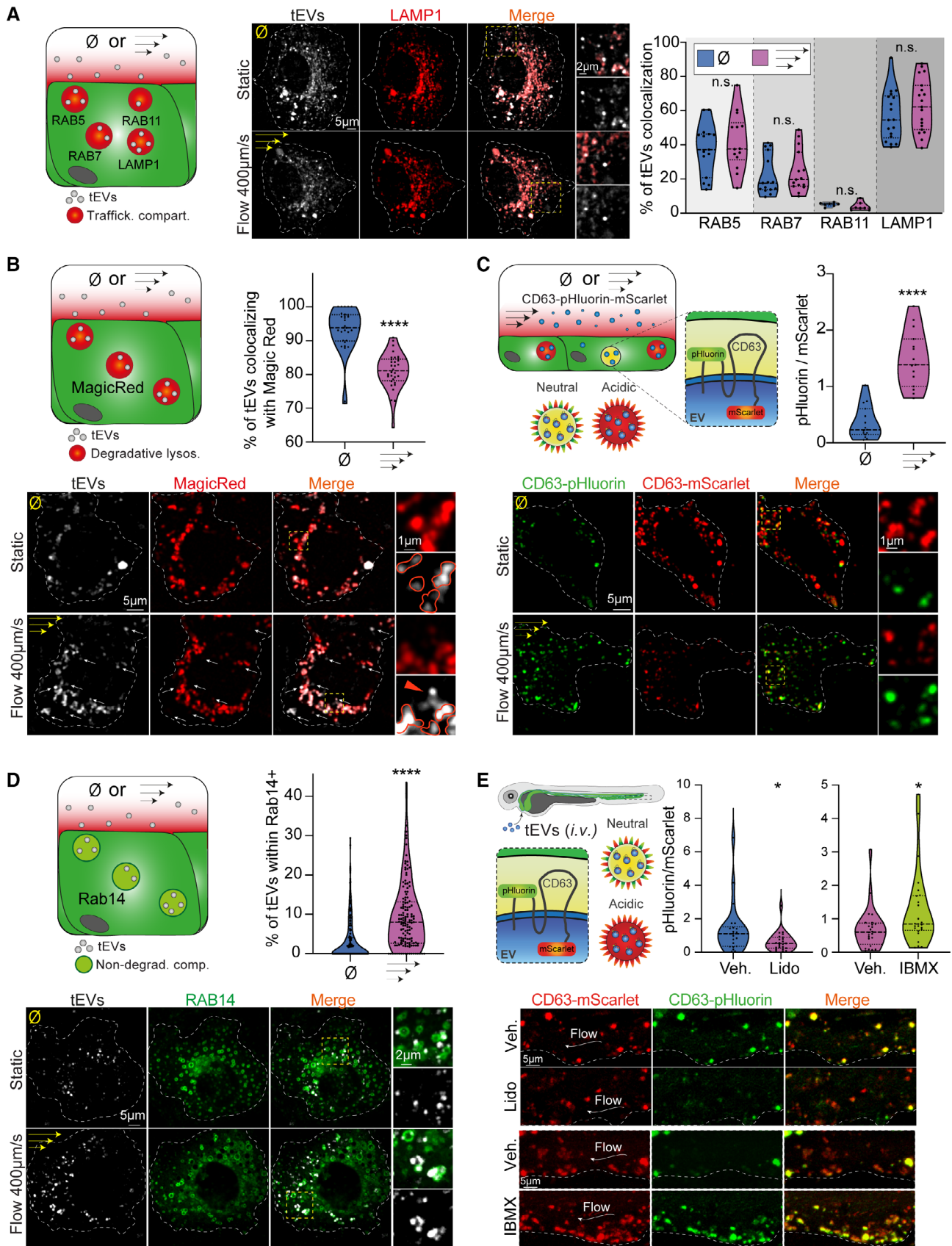


Figure 2.

luminal pH (Perera & Zoncu, 2016), we next probed the pH of tEV-containing compartments by exploiting the pH-sensitive reporter pHluorin. pHluorin is anchored on EVs external membrane via an insertion in the extracellular domain of the tetraspanin CD63, while the pH-insensitive mScarlet is fused to its intracellular C-terminal end (Sung *et al*, 2020). As pHluorin is fluorescent in a neutral environment but quenched in an acidic environment, it allows to probe the pH of the compartments targeted by tEVs (Fig 2C, left). We generated tumor cells expressing CD63-pHluorin-Scarlet and secreting pH-sensitive fluorescent EVs. The ratio of green (pHluorin) toward red (mScarlet) fluorescence was then used to probe the pH of tEVs' environment in receiving cells. When pH-sensor tEVs were perfused on endothelial cells, we again observed striking differences in endothelial cells subjected to flow. We found that flow drastically increased the pHluorin/mScarlet ratio (Fig 2C) suggesting that endothelial mechanosensing can change the trafficking routes of internalized tEVs and reroute them toward more neutral compartments. Together, these results show that internalized tEVs are in part diverted to less acidic and less degradative compartments when endothelial cells are cultured under low flow regimes.

In order to identify such compartments, we focused on Rab14, a Rab GTPase known for being localized in LAMP1 positive late endosomes, in addition to other compartments (Hoffman *et al*, 2022). Among other functions, Rab14 is involved in intracellular virus and pathogen trafficking towards late endo-lysosomes (Kyei *et al*, 2006; Kuijl *et al*, 2013; Okai *et al*, 2015). Importantly, Rab14 also controls the transit of internalized material toward non-acidic LAMP1 positive compartments (Trofimenko *et al*, 2021). Therefore, we stably expressed GFP-Rab14 in endothelial cells and first confirmed that Rab14 is mostly absent from lysosomal degradative compartments, as it only weakly co-localizes with Magic Red in static and flow conditions (Fig EV4). We then assessed whether tEVs traffic through Rab14 compartments. While internalized tEVs are often found in close proximity to Rab14 positive independently of flow, the proportion of tEVs within the lumen of Rab14 positive compartments is significantly increased in flow-stimulated endothelial cells (Fig 2D). Altogether, our results show that the low flow regimes partially

switch EVs trafficking, either directly or not, toward Rab14 positive non-acidic and non-degradative compartments suggesting that endothelial mechanosensing of flow would prevent some tEVs from degradation.

To validate our observations *in vivo*, we injected CD63-pHluorin-mScarlet tEVs in the circulation of zebrafish embryos where the flow speed was pharmacologically manipulated. We measured the pHluorin/mScarlet ratio of tEVs internalized in a single vessel (caudal vein) as performed in Fig 1 and observed that the pHluorin/mScarlet ratio was reduced in embryos with decreased flow velocities (Fig 2E), suggesting that tEVs accumulate *in vivo* in more acidic compartments under a reduced flow velocity. Conversely, increasing blood flow velocity with IBMX increases the pHluorin/mScarlet ratio, suggesting that tEVs tend to accumulate in less acidic compartments in endothelial cells facing higher flow speed. Altogether, our combined *in vitro* and *in vivo* data show that circulating tEVs follow a different trafficking route depending on hemodynamic forces applied on endothelial cells.

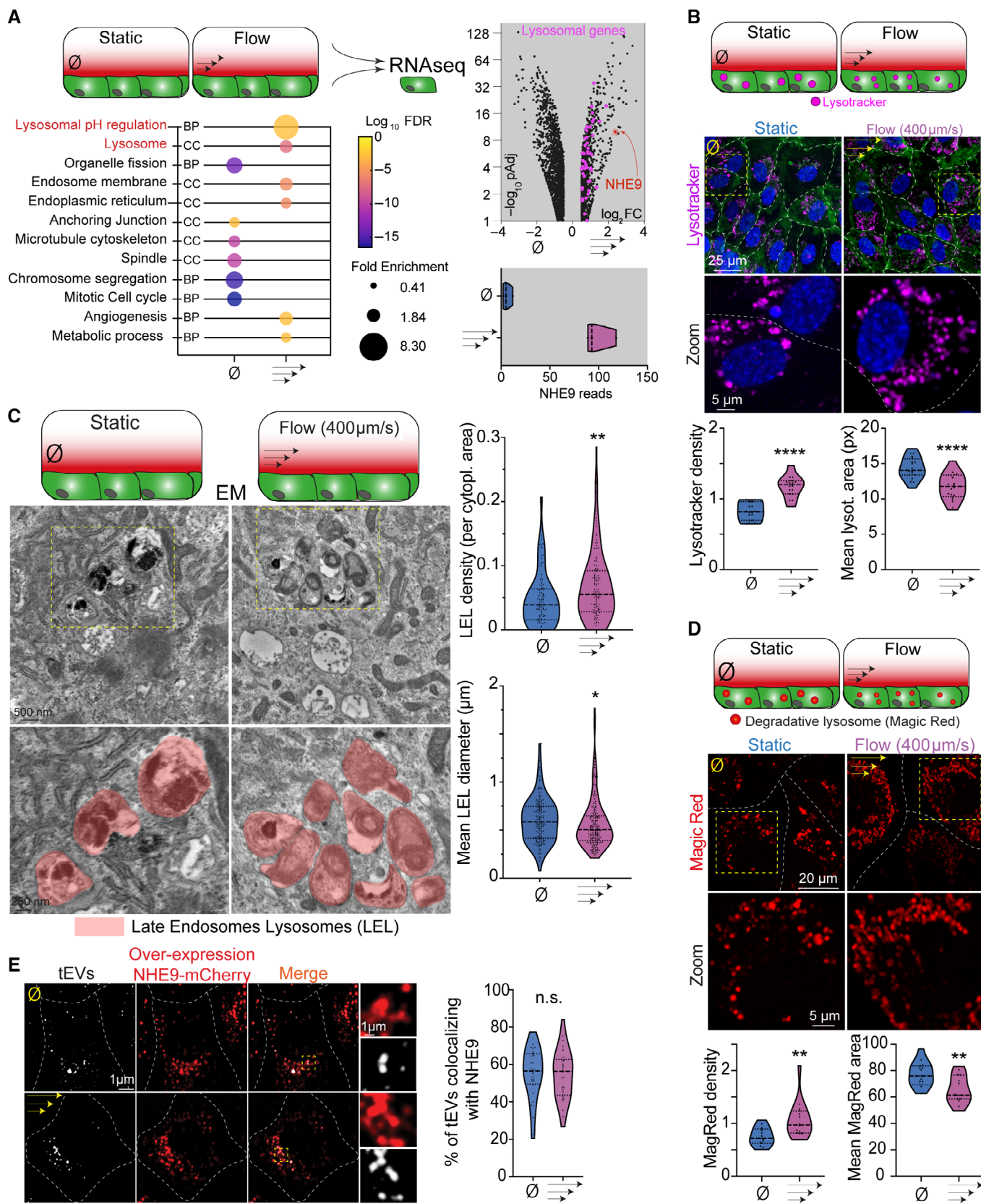
### Blood flow promotes lysosomal pathways in endothelial cells

Endothelial cells have exceptional mechanosensing abilities that orchestrate multiple cellular functions (Freund *et al*, 2012; Fang *et al*, 2019). Having observed that low flow regimes re-direct tEVs toward non-degradative compartments, we wondered whether this resulted from a broad re-organization of endosomal trafficking in flow-stimulated endothelial cells. To address this question, we analyzed endolysosomal trafficking in flow-stimulated endothelial cells, in absence of tEVs. We first compared transcriptional response using RNAseq in endothelial cells subjected to low flow (400  $\mu\text{m/s}$ ) or not (Dataset EV1). While earlier work had provided transcriptomic analysis of endothelial cells subjected to high-shear flow regimes (for example 10 dynes/cm<sup>2</sup>, García-Cardeña *et al*, 2001), we provide here an original documentation of the impact of low velocity flow regimes on endothelial transcriptional programs. Interestingly, such flow profiles significantly favor the transcription of genes associated with lysosomal pathways (Fig 3A). When probing

#### Figure 3. Blood flow upregulates lysosomal pathway.

- A RNA sequencing of HUVEC cells cultured under a moderate flow speed reveals an enrichment in genes associated with lysosomal regulation. Transcriptomics was performed on HUVEC cells cultured in static or flow conditions. The bubble plot shows the GO terms differentially expressed between static and flow conditions ( $P$ -values < 0.05 and  $\log_2$  fold-changes > 1; BP, biological process; CC, cellular components). The volcano plot shows the genes differentially expressed between static and flow conditions highlighting the 73 genes associated with lysosomes in pink and NHE9 in red. The lower right graph shows the number of NHE9 reads in static and flow conditions.
- B, C Increased number of lysosomes in endothelial cells cultured under flow and observed by photonic (B) and electronic microscopy (C). HUVEC cells were cultured in static or flow conditions, labeled with Memglow 488, Nucblue and lysotracker to visualize cells, nuclei, and lysosomes respectively and imaged by confocal as shown on representative maximum projection images. Left graph represents the relative number of lysosomes per cell and right graph the mean area of these compartments (one dot is one field of view,  $n = 20$  from two independent experiments,  $P < 0.0001$ , Student  $t$ -test comparing the density per field of view; lysot., lysotracker; Px, pixel) c Representative electron microscopy images of HUVEC cells cultured in flow and static conditions and schematic representation of late endosome lysosome (LEL, red). Graphs show an increase in the number of LEL per cytoplasmic surface (one dot represents one field of view;  $n = 121$  and 125 fields of view respectively;  $P = 0.0028$  Mann-Whitney) and a decrease in their average diameter in HUVEC cells cultured under flow (one dot represents one LEL;  $n = 166$  and 178 LELs respectively;  $P = 0.015$  Mann-Whitney). \* $P < 0.05$ ; \*\* $P < 0.01$ ; \*\*\*\* $P < 0.0001$ .
- D Increase in degradative compartments in HUVEC cells upon flow treatment. HUVEC cells were cultured in static or flow conditions, labeled Magic Red to visualize compartments with cathepsin B activity and imaged by confocal as shown on representative maximum projection images. Left graph represents the relative number of magic red positive compartment per cell (1 dot = 1 field of view (FOV);  $P = 0.0025$  Student  $t$ -test comparing the number of positive compartment per cell) and right graph the mean area of these compartments. (1 dot = 1 FOV  $P = 0.049$  Mann-Whitney) from two independent experiments. \*\* $P < 0.01$ .
- E NHE9 positive compartments accumulate tEVs. Representative confocal images (single plane) of internalized EVs in vHUVECs cells expressing NHE9-mCherry in flow or static conditions. Colocalization was quantified using an automated pipeline (Each dot represents one field of view,  $n = 34$ ; two independent experiments, Mann-Whitney comparing the colocalization per field of view,  $P = 0.6417$ ). n.s., non-significant.

Source data are available online for this figure.





the endolysosomal pathway using fluorescent dyes, we observed that flow increased the number of lysotracker positive compartments (Fig 3B). When carefully assessing inner trafficking compartments using electron microscopy, we confirmed that flow significantly increases the number of endolysosomes, which displayed a smaller mean size (Fig 3C) in agreement with fluorescence microscopy (Fig 3B), and that is directly linked to their degradative capacities (de Araujo *et al*, 2020). Therefore, to gain insight into the functionality of those compartments, we quantified the cathepsin B activity using the Magic Red dye. We observed that the number of Magic Red positive compartment is increased, while their apparent size is decreased (Fig 3D). This result suggests that endothelial cells sensing flow profiles that are permissive to tEVs uptake also increase their lysosomal degradative activity, which is regulated by pH. Altogether, these experiments show that flow profiles that do favor tEVs uptake and re-routing also promote endolysosomal degradative pathways. Therefore, the re-routing of EVs toward non-degradative compartments does not solely result from a mechano-transduction pathway that adjusts lysosomal pathways, but more likely reflects a flow-dependent EV specific switch in trafficking route. Interestingly, the RNAseq analysis further revealed that flow-stimulated endothelial cells activate expression of genes involved in the regulation of lysosomal pH, including the proton exchanger NHE9 (SLC9A9) which limits endosome luminal acidification (Fig 3A) (Kondapalli *et al*, 2015; Beydoun *et al*, 2017). We confirmed by independent RNA sequencing that flow triggers endogenous NHE9 expression and generated endothelial cells stably expressing NHE9-mCherry. Using these, we observed that fluorescent tEVs accumulate in NHE9-positive compartments (Fig 3E). Therefore, although we cannot exclude that flow impacts additional pathways, flow not only strengthens the lysosomal pathway in endothelial cells, through transcriptional control, it also triggers the formation of NHE9 compartments where tEVs accumulate.

### Blood flow and circulating tEVs cooperate to favor angiogenesis

Having demonstrated that low blood flow favors the lysosomal escape of tEVs, we wondered whether they might tune endothelial response. We first interrogated to what extent blood flow and tEVs would cooperate and impact transcriptional programs of targeted endothelial cells. Interestingly, the endothelial transcriptome was differentially impacted by tEVs in static and low flow condition

(Fig 4A and Dataset EV2). While the number of genes dysregulated by tEVs is similar in static and flow stimulated endothelial cells, their identity differs. Indeed, different sets of genes are transcriptionally impacted by tEVs when endothelial cells are cultured in static or low flow (Fig 4A, right). Among the genes upregulated by tEVs in flow-stimulated endothelial cells, we found several pro-angiogenic transcription factors, such as ID1, ID2, ID3, Hey1, Hey2, MAFB, Runx1 and HES1 (Benezra *et al*, 2001; Fischer *et al*, 2004; Kitagawa *et al*, 2013; Morioka *et al*, 2014). We further identified genes that are involved in two pro-angiogenic signaling pathways, the Notch (HEY1, HEY2, HES1, JAG1) and the TGF $\beta$  (Smad6, Smad7, Bambi, PMEPA1, Nog) pathways (Fig 4A, right). While the concerted action of flow and tEVs uptake in endothelial cells triggers activation of pro-angiogenic programs, possibly via the Notch and TGF $\beta$  pathways, whether they impact the angiogenic activity of endothelial cells remains unclear.

To test the relevance of this pro-angiogenic gene signature *in vivo*, we adapted a well-established experimental tumor angiogenesis assay in zebrafish embryos (Nicoli & Presta, 2007) to investigate whether tEVs could impact endothelial response in realistic hemodynamic conditions. To this end, we assessed the ability of intravenous injected and circulating tEVs to promote the formation of neo-sprouts from existing sub-intestinal vessels in embryos bearing a tumor mass. When embryos are injected with tEVs, the tumor-induced sprouting is potentiated with an increased number of neo-vascular sprouts per embryo (Fig 4B). Importantly, tEVs also increase the percentage of embryos bearing tumor-induced endothelial sprouts when compared to embryos injected with PBS. Together, our results demonstrate that circulating tEVs induce a pro-angiogenic response *in vivo*.

## Discussion

Overall, our work demonstrates for the first time that the fate and function of tEVs flowing in the bloodstream and on their way to shape pre-metastatic niches is tightly linked to hemodynamic forces and mechanosensing abilities of the endothelium. We provide here the first evidence that the endothelium uses its flow-sensing abilities to divert internalized tEVs from lysosomal degradation and thereby change their signaling capacities. We further identified the range of flow regimes where tEVs re-routing in venous endothelial cells is favored. In venous endothelial cells subjected to such flow regimes,

### Figure 4. Circulating tumor EVs and blood flow cooperate to promote angiogenesis.

- A RNA sequencing reveals an enrichment in pro-angiogenic pathways in HUVEC cells cultured under a moderate flow speed and treated with 4T1 tEVs. Transcriptomics was performed on HUVEC cells cultured in static or flow conditions and treated with 4T1 tEVs or PBS for 24 h. Heat map shows that the genes differentially expressed upon tEV treatment in flow condition are not deregulated in static conditions. The right graph shows differentially expressed genes, with increased (=Up) or decreased (=Down) expression with flow and/or tEVs ( $P_{Adj} < 0.1$ ). Pro-angiogenic transcription factors (=TFs) (orange) and members of the TGF $\beta$ /BMP pathway (green) are highlighted.
- B Tumor EVs promote angiogenesis *in vivo*. Zebrafish embryos were injected intravascularly (i.v.) with 4T1 tEVs or PBS and subsequently with 4T1 tumor cells (=TCs). Representative confocal images show neovascular sprouts in the sub-intestinal vessels (SIV) 24 h post-tumor cell injection. The number of neovascular sprouts (upper graph; one dot = one fish;  $n \sim 80$  embryos from five independent experiments; one-way ANOVA with Dunn's multiple comparison test, adjusted  $P$  value = 0.0001) and the percentage of embryos with neovascular sprouts (lower graph; one dot = one experiment; one-way ANOVA with Tukey's multiple comparisons; adjusted  $P$  values were as follows: CTL vs PBS + TCs  $P = 0.0186$ , CTL vs tEVs + TCs  $P < 0.0001$  and PBS + TCs vs tEVs + TCs  $P = 0.0156$ ) were quantified. Arrowheads point to neovascular sprouts. \* $P < 0.05$ ; \*\*\* $P < 0.001$ ; \*\*\*\* $P < 0.0001$ .
- C model explaining the fate and function of circulating tumor EVs: low flow speed promotes EVs uptake by endothelial cells followed by partial lysosomal escape and rerouting in RAB14 and NHE9 positive compartments. As a consequence, tumor EVs induce a pro-angiogenic response.

Source data are available online for this figure.

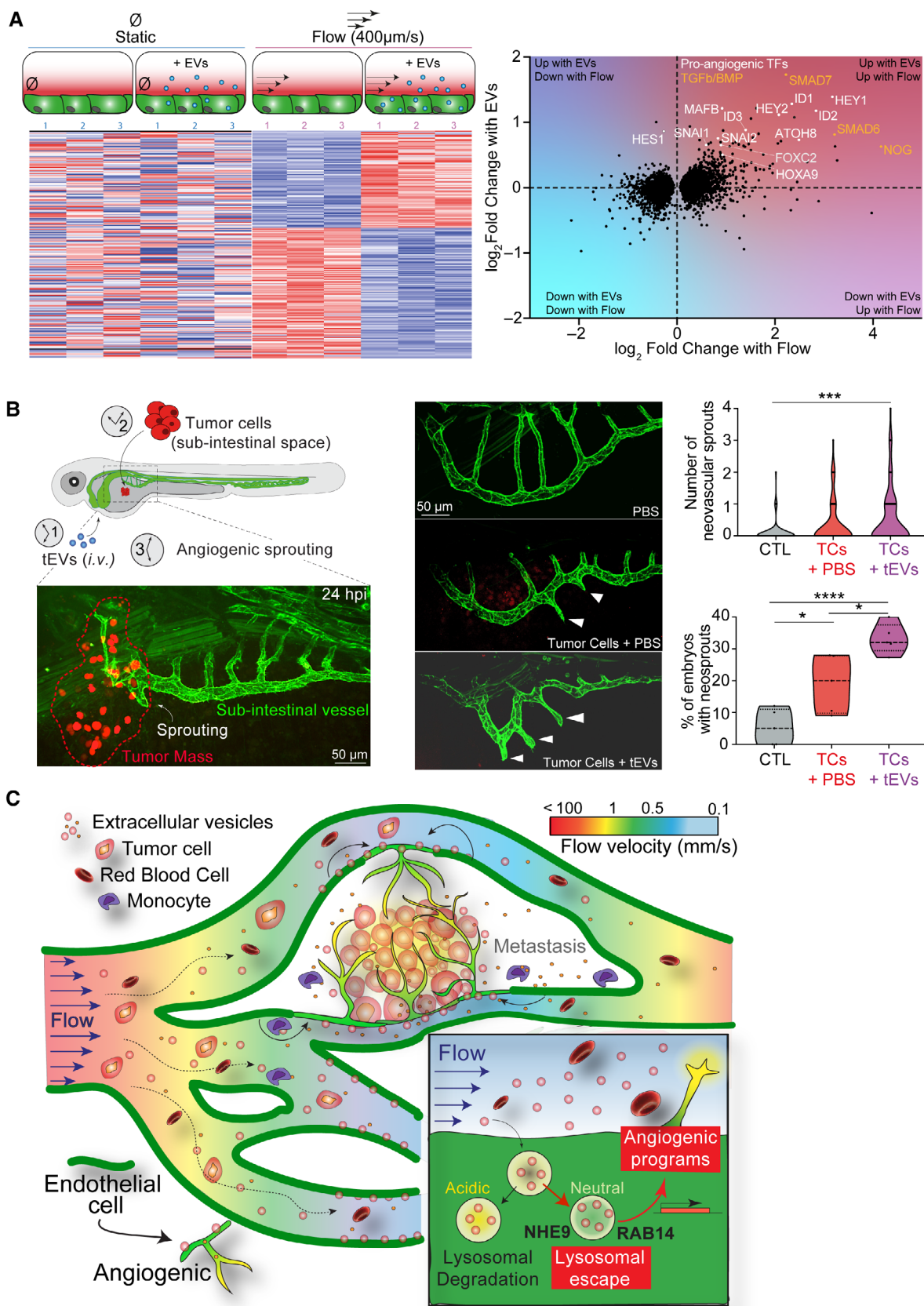


Figure 4.

internalized tEVs are partially re-routed to non-acidic and non-degradative RAB14 and NHE9 positive compartments with direct and functional consequences on their angiogenic potential. Such regimes not only favor the partial lysosomal escape of tEVs, they also allow the arrest of CTCs that precedes metastatic extravasation and outgrowth (Follain *et al*, 2018, 2020). Therefore, tEV-mediated indoctrination of endothelial cells and CTCs extravasation are likely to occur at similar locations, implying that CTCs would be prone to reach vessels that were already corrupted by tEVs. In addition to activating endothelial cells to favor arrest and extravasation of CTCs, tEVs are likely to favor the recruitment of immune cells to further support metastatic outgrowth. In conclusion, venous hemodynamics potentiate the functional impact of tEVs on endothelial cells toward a pro-angiogenic response which ultimately shapes pre-metastatic niches and metastatic outgrowth.

In this work, we propose that binding and arrest of tEVs at the endothelial surface is optimal in venous endothelial cells. We and others observed similar location of arrest using EVs of different origins (4T1 and AT3 triple-negative EVs in this study, zebrafish melanoma and fibroblast EVs in a previous study (Hyenne *et al*, 2019), RBC and endothelial EVs in two recent independent studies (Qin *et al*, 2022; preprint: Coly *et al*, 2023)). Interestingly, similar observations were made with synthetic nanoparticles as their uptake by endothelial cells is higher at venous-like low shear stress than in static conditions, but decreases at higher arterial-like shear stress in a receptor-dependent manner (Lin *et al*, 2010; Han *et al*, 2012, 2015; Chen *et al*, 2020). While our results certainly demonstrate that flow forces reroute EVs within endothelial cells, flow tuning had no effect on the ratio of uptake measured in the dorsal aorta vs. the caudal vein (Fig EV2C). Besides, drastically increasing the magnitude of flow *in vitro* (4400  $\mu\text{m}/\text{S}$ ) had no further effect on the total amount of internalized EVs, yet it led to a heterogeneous pattern of uptake with many cells internalizing big amounts of EVs (Fig EV2D). The precise nature of the mechanisms involved in the internalization of circulating EVs remain however to be determined. Interestingly, we had observed EVs rolling on the surface of the caudal vein endothelium of zebrafish embryos at low flow velocity (Hyenne *et al*, 2019), suggesting direct receptor-mediated interactions between EVs and the endothelial surface. We and others had shown that endothelial targeting of tEVs also relies on specific adhesion receptors present at their surface, such as integrins or CD146/MCAM (Hoshino *et al*, 2015; Ghoroghi *et al*, 2021b; Jerabkova-Roda *et al*, 2022). Therefore, expression of these receptors at the surface of subtypes of EVs or on EVs from different origins could also account for different uptake patterns. While the identity of the ligands of such receptors remains obscure, their differential expression with respect to endothelial cells identity (or in different organs) could also contribute to EV biodistribution. In some organs, such as the liver, venous endothelial cells are specialized in the uptake of circulating macromolecules and small lipid-based structures through the expression of specific cell surface receptors (Pandey *et al*, 2020). Therefore, we propose that the destination of circulating tEVs relies on the combined effect of hemodynamics, vessel identity and receptor-ligand interactions. Our results also show that at moderate velocities, internalized tEVs are partially rerouted toward non-acidic compartments suggesting that the fate of tEVs, and their function, is controlled by the mechanosensing abilities of the endothelium. Flow-dependent trafficking of internalized tEVs could determine the proportion of EVs undergoing

lysosomal degradation and tEVs allowed to transfer their cargo through back-fusion in endosomes. However, since both processes rely on endosomal acidification (Joshi *et al*, 2020; Bonsergent *et al*, 2021), the extent to which tEVs escape lysosomal degradation could relate to alternative fate, such as direct signaling from endosomes (Shelke *et al*, 2019) or endothelial transcytosis which allows tEVs to cross the blood–brain barrier (Morad *et al*, 2019). Characterizing the proportion of internalized EVs following each of these fates will be essential in the future and would require the development of innovative *in vivo* compatible tools.

Flow forces favor lysosomal escape allowing tEVs to promote a pronounced pro-angiogenic transcriptional program in endothelial cells. Flow mechanotransduction could act in two ways: either it impacts cargo transfer or it tunes the interpretation of EV signaling by endothelial cells. When subjected to flow, EVs trigger the activation of the TGF $\beta$  and Notch pathways. How tEVs activate these pathways remains unclear, yet we found that 4T1 tEVs contain several regulators of the TGF $\beta$  pathway (Smad5, Smurf2, etc.) (Ghoroghi *et al*, 2021b), including TGF $\beta$  type II receptor, whose presence on tEVs is sufficient to trigger the pathway in receiving cells (Xie *et al*, 2022). Mechanistically, both the TGF $\beta$  pathway, as well as the Notch pathway can also be activated directly from endosomes (Baron, 2012), and possibly from internalized tEVs (Shelke *et al*, 2019). Activation of this pro-angiogenic program, potentially through Notch and TGF $\beta$  pathways, could impact metastasis in many ways. Activation of Notch1 in endothelial cells of the pre-metastatic niche, for instance, favors neutrophils infiltration and ultimately metastasis (Wieland *et al*, 2017). Besides, endothelial tEVs were shown to activate the Notch pathway in endothelial cells, resulting in increased expression of HEY1 and HEY2 and formation of capillary-like structures *in vitro* and *in vivo* (Sheldon *et al*, 2010). In addition, activation of the TGF $\beta$  pathway in endothelial cells promotes inflammation and endothelial permeabilization (Chen *et al*, 2019), while the presence of TGF $\beta$  type II receptor on tEVs correlates with metastasis (Xie *et al*, 2022). While it remains unclear whether and how the positive impact of tEVs on sprouting efficacy of the endothelium impacts metastasis progression, we speculate that it acts as an initial trigger of the priming of metastatic niches or of the vascularization of metastatic foci. Indeed, circulating tEVs promote tumor-induced neo-angiogenesis *in vivo*, a scenario that is likely to happen when tEVs shape pre-metastatic niches (Peinado *et al*, 2017; Ghoroghi *et al*, 2021a). While tumor tEVs were previously shown to promote angiogenesis *in vitro* (Todorova *et al*, 2017), our results suggest that such effect can be potentiated by hemodynamic forces of perfused vessels. As a consequence, we expect circulating tEVs to favor the formation of neo-vascular sprouts in capillary-like vessels that are prone, from a hemodynamics stand-point, to the arrest of CTCs (Follain *et al*, 2018). The formation of new and abnormal blood vessels could constitute a first step in the creation of pre-metastatic niches, leading to the subsequent recruitment of specific immune populations and ultimately favoring homing of circulating tumor cells (Peinado *et al*, 2017). We have recently shown that endothelial cells also hijack a flow-stimulated pro-angiogenic transcriptional program to perform intravascular remodeling that favors the extravasation of arrested CTCs (Follain *et al*, 2018, 2021). It is thus tempting to speculate that tEVs could mediate such intravascular remodeling, whose dependence on flow forces is also established (Follain *et al*, 2021). Finally, one

could expect that tEVs are continuously secreted after metastasis initiation, leading to the induction of neo-sprouts which sustain the growth of metastatic foci that have colonized distant organs (Kienast *et al*, 2010).

## Material and Methods

### Cell culture

4T1 cells (4T1 native, 4T1 CD63-APEX2-GFP, 4T1 CD63-pHluorin-mScarlet and 4t1-NLS-tdTomato-IH) and AT3 cells were cultured in RPMI-1640 medium complemented with 10% Foetal Bovine Serum (FBS, Hyclone) and 1% penicillin/streptomycin (PS, 100 U/ml, Gibco). HUVEC cells (Human Umbilical Vein Endothelial Cell, Promocell) were grown in Endothelial Growth Medium (ECGM, Promocell) complemented with supplemental mix (SupplementMix, Promocell) and 1% PS. Veravec™ are HUVECs human endothelial cells adapted to longer term culture using a single adenovirus protein, E4ORF1 (Angiocrine Biosciences). They were cultured in ECGM MV2 (Promocell) complemented with 20% of FBS and 1% PS. For all the microfluidic experiments, HUVECs or vHUVECs were used before passage number 4. HEK293T cells were grown in DMEM (Gibco) complemented with 10% FBS and 1% PS. All cell lines were maintained at 37°C and 5% CO<sub>2</sub> and verified for the absence of mycoplasma by PCR on a regular basis.

### Stable cell line generation

Lentivirus containing the following constructs were produced in HEK293T cells using JetPRIME (Polyplus, FRANCE) transfection: pLSFFV-mCherry-Rab5A, pLSFFV-RFP-LAMP1, pLSFFV-mEmerald-Rab7A, pLSFFV-eGFP-Rab11A, pLSFFV-GFP-Rab14 (gift from N. Vitale, INCI, Strasbourg, France), pLSFFV-NHE9-mCherry (gift from K. C. Kondapalli, Michigan-Dearborn University, USA), pLSFFV-CD63-APEX2-GFP, pLSFFV-pHluorin-CD63-mScarlet (gift from A. M. Weaver, Vanderbilt University, USA) together with packaging expression vectors pLP1, pLP2 and pLP3. vHuvec or 4T1 cells were infected by lentivirus in the presence of 5 µg/ml polybrene (Sigma) followed by antibiotic selection (Puromycin at 1 µg/ml or blasticidin at 5 µg/ml).

### EVs isolation and labeling

4T1 EVs were previously characterized by electron microscopy, nanoparticle tracking analysis, proteomics and Western blots (Hyenne *et al*, 2015; Ghoroghi *et al*, 2021b). In brief, cells were cultured at sub-confluency in EV depleted medium for 24 h. EV depleted medium was prepared using 2× complete medium, centrifuged at 100,000 g for 20 h (Optima XE-90 ultracentrifuge—Beckman Coulter) to eliminate EVs from FBS. Supernatant was then filtered at 0.22 µm (Millipore) and adjusted to 1×. tEVs were mostly isolated using differential ultracentrifugation protocols as described previously (Hyenne *et al*, 2015, 2019). The pellets obtained at the final step of 100,000 g centrifugation were resuspended in sterile PBS1X. In Fig EV2A, EVs were isolated by size exclusion chromatography (SEC) using the iZON qEV2 size exclusion column (Izon science, Cambridge MA) according to the manufacturer's instructions

and as previously described (Ghoroghi *et al*, 2021b). In brief, 2 ml of concentrated extracellular medium were applied on top of a qEV column and 6 ml fractions were collected. Four EV-rich fractions (F2, F4, F6, and F8) were pooled, then concentrated using an Amicon Ultra-4 10 kDa centrifugal filter device (Merck Millipore). Pellets were resuspended in 500 µl PBS. When needed, tEVs were labeled using 200 nM of MemGlow-Cy5 (Cytoskeleton Inc.) lipidic dye between the 1<sup>st</sup> and the 2<sup>nd</sup> 100,000 g ultracentrifugation as described previously (except for SEC where labeled EVs were concentrated with an Amicon Ultra-4-10 kDa). Following the tEV isolation, their number and size distribution were measured by ZetaView NTA (PMX-120-12B-R2—Particle Metrix). tEVs were stored at 4°C and used within 24 h.

### Microfluidics experiments

For microfluidic experiments, IBIDI® µ-slides with 1 (µ-Slide I 0.4 Luer ibiTreat: #1.5 polymer coverslip) or 6 (µ-Slide VI 0.4 ibiTreat: #1.5 polymer coverslip) channels were coated with fibronectin (SIGMA) for 1 h and seeded with 100,000 or 50,000 cells per channel respectively. Once endothelial cells reached confluency, the channels were either maintained in static conditions or continuously perfused under a flow of 400 µm/s for 17 h using a Reglo Digital MS-CA 2/12 peristaltic pump. tEVs were then either applied on the static cells or perfused continuously under flow at a concentration of  $5 \times 10^8$  to  $1 \times 10^9$  particles/ml. After 3 h of tEV perfusion, channels were removed from the flow, and washed 3 times with fresh ECGM and 3 times with ECGM/Hoechst 33342 (NucBlue™ ThermoFisher). After 10 min incubation, cells were washed twice with ECGM/HEPES 20 mM before imaging. To assess lysosome number or Cathepsin-B activity, endothelial cells were incubated after EV perfusion with LysoTracker Deep Red (Thermo Fisher Scientific) diluted at 50 nM or MagicRed dye (Bio-Rad) diluted at 1:260 respectively for 1 h. When needed, cells were incubated with MemGlow-488 (Cytoskeleton Inc.) at 200 nM to label the plasma membrane.

### Photonic microscopy and image analysis

Cells were imaged live at 37°C with 5% CO<sub>2</sub> with an Olympus Spinning Disk (60× objective, N.A. 1.2), with a Leica SP5 confocal (63× objective, N.A. 1.25) or with a Zeiss LSM 800 confocal (63× objective, N.A. 1.4). Zebrafish embryos were imaged live at 28°C with a Leica SP5 confocal equipped with a HC PL APO 20X/0.7 IMM objective or with an Olympus Spinning Disk equipped with a 30× objective (N.A. 1.05). Image analysis and processing were performed using the Fiji (2.0.0) (Schindelin *et al*, 2012), Cell Profiler (4.2.1) (Stirling *et al*, 2021) and ICY (2.4.2.0.) (De Chaumont *et al*, 2012) software. Number, intensity, and area of compartments (Figs 1D and 3B and D) were quantified on maximum intensity projections using the ICY Spot detector plugin. To quantify tEV signal in the endothelium *in vivo* (Fig 1B and C), we used an in-house built Fiji macro to quantify the total tEV fluorescence in the tail region and specifically in the endothelium. Colocalization (Figs 2A, B and D, and 3E and EV2) was analyzed on processed single Z planes (Despeckle and Gaussian blur filter in Fiji) based on intensity thresholding using Cell Profiler. Areas of overlapping regions between tEVs and given compartment were quantified. The

percentage of tEV colocalization with the given compartment was calculated as a ratio of tEV overlap area to the total area of tEV objects times 100. The *in vitro* CD63-pHluorin/mScarlet experiments (Fig 2C), were analyzed on processed single planes, using masks to detect single spots and measure fluorescence intensities in the endothelium. For each field of view, total green and red spots fluorescence was then measured and used to calculate a pHluorin/mScarlet ratio. For the *in vivo* CD63-pHluorin/mScarlet experiments (Fig 2C), the venous endothelium was first manually segmented and the total green and red spots fluorescence in the endothelium was then measured on thresholded single Z planes and used to calculate a pHluorin/mScarlet ratio.

### Electron microscopy

**Chemical fixation:** Cells were fixed with 2.5% glutaraldehyde (GA)/2.0% paraformaldehyde (PFA) (Electron Microscopy Sciences) in 0.1 M NaCac buffer (pH 7.4) at RT for 2 h, then rinsed in 0.1 M NaCac buffer (pH 7.4) (Electron Microscopy Sciences) and post-fixed with 1% OsO<sub>4</sub> (Electron Microscopy Sciences) and 0.8% K<sub>3</sub>Fe(CN)<sub>6</sub> (Sigma-Aldrich) for 1 h at RT. Then, samples were rinsed 0.1 M NaCac buffer (pH 7.4) followed by a distilled water rinse and stained with 1% uranyl acetate, overnight at 4°C sheltered from the light.

The samples were stepwise dehydrated in Ethanol (50% ×10 min, 70% ×10 min, 95% ×15 min and 100% 3 × 10 min), infiltrated in a graded series of Epon (Ethanol 100%/Epon 3/1, 1/1) 1 h and kept in Ethanol 100%/Epon 1/3 overnight at RT. The following day, samples were placed in pure Epon 3 × 1 h and polymerized at 60°C 48 h. 100 nm thin sections were collected in 200 copper mesh grids and data set was acquired with a TEM Hitachi 7500 TEM, with 80 kV beam voltage, and the 8-bit images were obtained with a Hamamatsu camera C4742-51-12NR.

The number of MVBs and lysosomes per surface of cytoplasm were quantified using the Fiji software. MVBs and late endosome lysosomes were distinguished based on their morphology: MVBs have one or more ILVs and late endosome lysosomes contain ILVs but are also electron dense and contain irregular membrane curls.

### Intravascular injection of tEVs in zebrafish embryos

Zebrafish embryos were obtained from the following strains: *Tg (fli1a:eGFP)*, *Tg (fli: LA-eGFP)*, *Tg (fli:Gal4; UAS:RFP)*, *Casper Tg (Gata1:RFP; flk:GFP)*. Embryos were maintained at 28°C in Danieau 0.3× medium, supplemented with 1-Phenyl-2-thiourea (PTU, Sigma-Aldrich) after 24 h post fertilization (hpf). All injection experiments were carried out at 48 hpf and imaged between 48 and 72 hpf. All animal procedures were performed in accordance with French and European Union animal welfare guidelines and supervised by local ethics committee (Animal facility #A6748233; APAFIS #2018092515234191). At 48 hpf, zebrafish (ZF) embryos were dechorionated and mounted on a 0.8% low melting agarose pad containing 650 μM tricaine (ethyl-3-aminobenzoate-methanesulfonate). Embryos were injected intravascularly in the duct of Cuvier with 27.6 nl of MemBright Cy5- labeled tEVs or 4T1CD63pHluorinmScarlet-tEVs (at 10<sup>10</sup> EVs/ml) with a Nanoject microinjector 2 (Drummond) under a M205 FA stereomicroscope (Leica) as described previously (Hyenne et al, 2019; Mary et al, 2020).

### Sample preparation for correlative light and electronic microscopy of ZF embryos

Correlative Light and Electron Microscopy was performed as previously described (Hyenne et al, 2019; Mary et al, 2020). Transgenic *fli1:GFP* embryos were injected with MemGlow-Cy3 tEVs and imaged alive with a Leica SP8 confocal microscope. Z stack was performed on the caudal vein regions that had internalized EVs. After imaging, the embryo was chemically fixed with 2.5% glutaraldehyde and 4% paraformaldehyde in 0.1 M Cacodylate buffer (the fish tail was cut off in the fixative). The sample was kept in fixative at RT for 1–2 h and stored in fixative at 4°C overnight until further processing. The sample was rinsed in 0.1 M Cacodylate buffer for 2 × 5 min and post-fixed using 1% OsO<sub>4</sub> in 0.1 M Cacodylate buffer, for 1 h at 4°C. Then, sample was rinsed for 2 × 10 min in 0.1 M Cacodylate buffer and secondary post-fixed with 4% water solution of uranyl acetate, 1 h at RT. Rotation was used at all steps of sample processing. Followed by 5 min wash in MiliQ water, the sample was stepwise dehydrated in Ethanol (25%, 50% each 15 min, 95%, 3 × 100% each 20 min) and infiltrated in a graded series of Epon (Ethanol/Epon 3/1, 1/1, 1/3, each 45 min). Sample was left in absolute Epon (EmBed812) overnight. The following day, sample was placed in a fresh absolute Epon for 1 h and polymerized (flat embedded) at 60°C for 24–48 h. Once polymerized, most surrounding Epon was cut off using razorblade and sample was mounted on empty Epon blocks (samples flat on the top of the blocks) and left at 60°C for 24 h–48 h. The region of interest was targeted by ultramicrotome, sections and compared with the LM datasets. After targeting, serial 100 nm sections were collected in formvar coated slot grids. The sections were post stained with uranyl acetate (4%) and lead citrate. The sections were imaged in a Biotwin CM120 Philips (FEI) TEM at 80 kV with a SIS 1 K Keen-View. Stiches of the 70 sections were aligned using the Track EM plugin in Fiji (Cardona et al, 2012).

### Blood flow mapping

For flow speed mapping, we injected MemGlow labeled 4 T1 tEVs in *Tg (kdrl:EGFP; gata1:DsRed)* embryos in Casper background at 48 hpf. 30 min post injection, we recorded short time-lapses in four different regions in the zebrafish caudal plexus (two in the dorsal aorta and two in the venous area) using spinning disk. For each region, we recorded 30 s time-lapses (17 ms time interval) at single focal plane with flowing red blood cells (RBC). Flow speed was measured by tracking RBC in each region with IMARIS software (v9.5.1) (using spot detection method and tracking algorithm in autoregressive motion). tEVs (Cy5) accumulation in endothelial cells (GFP) was measured by IMARIS for each region.

### Pharmacological blood flow tuning

IBMX (3-Isobutyl-1-Methylxanthin—15879—Merck) and lidocaine (L7757—Merck) were directly added to the embryo water (Danieau/PTU solution) containing ZF embryos at the concentration of 100 μM in DMSO for 20 h and at the concentration of 640 μM in EtOH for 2 h respectively. Control embryos were treated with similar amount of DMSO or EtOH accordingly. Embryos were then mounted and maintained in fresh solutions of drugs until the end of

the experiment. Heartbeat of the embryos were recorded as short time-lapses with a Stereomicroscope (Leica M205 FA). Heartbeats were manually counted on kymographs.

### In vivo angiogenesis assay

PTU treated *Tg(Fli: LA-eGFP)* dechorionated embryos were either uninjected (control) or injected with PBS or with 4T1 Memglow-labeled tEVs at 36 hpf intravascularly. At 48 hpf, PBS injected and tEV injected embryos received 4T1-NLS-tdTomato-IH tumor cell injection (volume-18 nl containing ~ 100–150 cells) in the perivitelline space. 24 hpi of tumor cells embryos were imaged by spinning Disk focusing on the sub-intestinal vein (SIV) plexus (that spans the dorso-lateral part of the yolk) as described in (Hen et al, 2015). The number of newly formed vascular sprouts was manually counted.

### Transcriptomic analyses

Transcriptomics from Fig 4A was performed on HUVECs cultured in static or flow conditions and treated with  $1 \times 10^9$  EVs or PBS for 24 h, while transcriptomics from Fig 3A was performed on HUVECs as described previously (Follain et al, 2021).

### RNA extraction and sequencing

Total RNA was extracted using RNeasy Mini Kit (Qiagen, Hilden, Germany) and RNA integrity was assessed by Bioanalyzer (total RNA Pico Kit, 2100 Instrument, Agilent Technologies, Palo Alto, USA). SMART-Seq® HT PLUS Kit (Takara, Kusatsu, Japan) was used to build mRNA libraries. Libraries were pooled and sequenced (single-end, 75 bp) on a NextSeq500 using the NextSeq 500/550 High Output Kit v2 according to the manufacturer's instructions (Illumina Inc., San Diego, CA, USA).

### Analysis of RNA-sequence reads: identification of differentially expressed genes

Sequence reads were mapped on the human hg19 genome using STAR (Dobin et al, 2012) to obtain a BAM file (Binary Alignment Map). Raw read counts were determined as an abundance matrix with the HTseq-count tool of the Python package HTSeq (Anders et al, 2014). Trimmed Mean of *M*-values normalization (TMM) was applied using the EdgeR package (Robinson et al, 2009). A voom transformation was applied to the data that were then fitted into a linear model using weighted least squares for each gene with limma package (Ritchie et al, 2015). Finally, a contrast matrix was created and differential expressions were computed. Up- and down-regulated genes were selected based on adjusted *P*-values < 0.05 and  $\log_2$  fold-changes > 1 for Fig 3A and on adjusted *P*-values < 0.1 and  $\log_2$  fold-changes > 0.5 for Fig 4A. The later analysis uses looser thresholds to take into account the double analysis (+/- Flow, +/- EVs). Functional enrichment analyses were performed using STRING v11 (Szklarczyk et al, 2019) and Gene Ontology (Carbon et al, 2021).

### Statistical analysis

All experiments were performed in two to three independent experiments. Statistical analysis of the results was done using GraphPad Prism (Software version 9.0). Normality of the data was confirmed

using Shapiro-Wilkson test and accordingly different statistical tests were used as described in legends. For data that follow gaussian distribution, unpaired *t*-test or one-way ANOVA (with Tukey's post-test analysis) were used. For data that do not follow gaussian distribution, Mann-Whitney or Kruskal-Wallis tests (with Dunn's post-test analysis) were used. Illustrations of the statistical analyses were displayed in the figures as the mean  $\pm$  standard deviation (SD). *P*-values smaller than 0.05 were considered as statistically significant. \**P* < 0.05, \*\**P* < 0.01, \*\*\**P* < 0.001, \*\*\*\**P* < 0.0001.

## Data availability

The RNAseq dataset produced in this study is available in ArrayExpress (accession E-MTAB-13156), <http://www.ebi.ac.uk/arrayexpress/experiments/E-MTAB-13156>. Data sources are available through this link: <https://www.ebi.ac.uk/biostudies/studies/S-BSST1174?key=bb5b5bd3-8849-4cce-ac0e-840b86ce322d>.

**Expanded View** for this article is available [online](#).

## Acknowledgements

We thank all members of the Goetz Lab for helpful discussions, in particular Florent Colin for careful reading, Naël Osmani and Gautier Follain for early interaction on HUVEC analysis, Nina Fekonja for EM assistance and Amandine Dupas for unpublished experiments. We thank Pascal Kessler (PICSTRA, CRBS) for assistance in imaging and image analysis, Coralie Spiegelhalter (IGBMC, Strasbourg, France) and Cathy Royer (INCI, Strasbourg, France) for assistance in EM imaging as well as Gregory Khelifi and Camille Hergott for animal care. We are grateful to Nicolas Vitale (INCI, Strasbourg, France), K. C. Kondapalli (Michigan-Dearborn University, USA) and A. M. Weaver (Vanderbilt University, USA) for sharing constructs. This work was supported by a fourth-year thesis and a post-doctoral fellowship from la Fondation pour Recherche Medicale (FRM) to BM and KJR respectively; by grants from La Ligue contre le Cancer, Cancéropôle Grand-Est, INCA (PLBIO19-291) and French National Plan Cancer (Vesmatic) and from the Programme Fédérateur Aviesan (Nanotumor) to VH and JGG; and by institutional funds from University of Strasbourg and INSERM.

## Author contributions

**Benjamin Mary:** Formal analysis; investigation. **Nandini Asokan:** Formal analysis; investigation. **Katerina Jerabkova-Roda:** Formal analysis; investigation. **Annabel Larnicol:** Formal analysis; investigation. **Ignacio Busnelli:** Investigation. **Tristan Stemmen:** Investigation. **Angélique Pichot:** Investigation. **Anne Molitor:** Investigation. **Raphaël Carapito:** Supervision. **Olivier Lefebvre:** Investigation. **Jacky G Goetz:** Conceptualization; supervision; funding acquisition; writing – original draft; writing – review and editing. **Vincent Hyenne:** Conceptualization; formal analysis; supervision; funding acquisition; investigation; writing – original draft; writing – review and editing.

## Disclosure and competing interests statement

The authors declare that they have no conflict of interest.

## References

Anders S, Pyl PT, Huber W (2014) HTSeq—a Python framework to work with high-throughput sequencing data. *Bioinformatics* 31: 166–169

- de Araujo MEG, Liebscher G, Hess MW, Huber LA (2020) Lysosomal size matters. *Traffic* 21: 60–75
- Baron M (2012) Endocytic routes to Notch activation. *Semin Cell Dev Biol* 23: 437–442
- Benezra R, Rafii S, Lyden D (2001) The Id proteins and angiogenesis. *Oncogene* 20: 8334–8341
- Beydoun R, Hamood MA, Gomez Zubieta DM, Kondapalli KC (2017) Na<sup>+</sup>/H<sup>+</sup> exchanger 9 regulates iron mobilization at the blood-brain barrier in response to iron starvation. *J Biol Chem* 292: 4293–4301
- Bonsergent E, Grisard E, Buchrieser J, Schwartz O, Théry C, Lavieu G (2021) Quantitative characterization of extracellular vesicle uptake and content delivery within mammalian cells. *Nat Commun* 12: 1–11
- Carbon S, Douglass E, Good BM, Unni DR, Harris NL, Mungall CJ, Basu S, Chisholm RL, Dodson RJ, Hartline E et al (2021) The Gene Ontology resource: enriching a GOLD mine. *Nucleic Acids Res* 49: D325–D334
- Cardona A, Saalfeld S, Schindelin J, Arganda-Carreras I, Preibisch S, Longair M, Tomancak P, Hartenstein V, Douglas RJ (2012) TrakEM2 software for neural circuit reconstruction. *PLoS One* 7: e38011
- Chen PY, Qin L, Li G, Wang Z, Dahlman JE, Malagon-Lopez J, Gujja S, Cilfone NA, Kauffman KJ, Sun L et al (2019) Endothelial TGF- $\beta$  signalling drives vascular inflammation and atherosclerosis. *Nat Metab* 19: 912–926
- Chen YY, Syed AM, MacMillan P, Rocheleau JV, Chan WCW (2020) Flow rate affects nanoparticle uptake into endothelial cells. *Adv Mater* 32: 1–7
- Cheng L, Hill AF (2022) Therapeutically harnessing extracellular vesicles. *Nat Rev Drug Discov* 215: 379–399
- Collot M, Ashokkumar P, Anton H, Boutant E, Faklaris O, Galli T, Mély Y, Danglot L, Klymchenko AS (2018) MemBright: a family of red to near-infrared fluorescent membrane probes for advanced cellular imaging and neuroscience. *Cell Chem Biol* 26: 600–614
- Coly P-M, Chatterjee S, Mezine F, El Jekmek C, Devue C, Nipoti T, Corona ML, Dingli F, Loew D, van Niel G et al (2023) Atheroprone shear stress stimulates noxious endothelial extracellular vesicle uptake by MCAM and PECAM-1 cell adhesion molecules. *bioRxiv* <https://doi.org/10.1101/2022.12.31.522373> [PREPRINT]
- De Chaumont F, Dallongeville S, Chenouard N, Hervé N, Pop S, Provoost T, Meas-Yedid V, Pankajakshan P, Lecomte T, Le Montagner Y et al (2012) Icy: an open bioimage informatics platform for extended reproducible research. *Nat Methods* 9: 690–696
- Dobin A, Davis CA, Schlesinger F, Drenkow J, Zaleski C, Jha S, Batut P, Chaisson M, Gingeras TR (2012) STAR: ultrafast universal RNA-seq aligner. *Bioinformatics* 29: 15–21
- Fang Y, Wu D, Birukov KG (2019) Mechanosensing and mechanoregulation of endothelial cell functions. *Compr Physiol* 9: 873
- Fischer A, Schumacher N, Maier M, Sendtner M, Gessler M (2004) The Notch target genes Hey1 and Hey2 are required for embryonic vascular development. *Genes Dev* 18: 901–911
- Follain G, Osmani N, Sofia A, Allio G, Mercier L, Karreman MA, Solecki G, Leon MG, Lefebvre O, Fekonja N et al (2018) Hemodynamic forces tune the arrest, adhesion and extravasation of circulating tumor cells. *Dev Cell* 45: 33–52
- Follain G, Herrmann D, Harlepp S, Hyenne V, Osmani N, Warren SC, Timpson P, Goetz JG (2020) Fluids and their mechanics in tumour transit: shaping metastasis. *Nat Rev Cancer* 20: 107–124
- Follain G, Osmani N, Gensbittel V, Asokan N, Larnicol A, Mercier L, Garcia-Leon MJ, Busnelli I, Pichot A, Paul N et al (2021) Impairing flow-mediated endothelial remodeling reduces extravasation of tumor cells. *Sci Rep* 11: 1–15
- Freund JB, Goetz JG, Hill KL, Vermot J (2012) Fluid flows and forces in development: functions, features and biophysical principles. *Dev* 139: 3063
- García-Cardena G, Comander J, Anderson KR, Blackman BR, Gimbrone MA (2001) Biomechanical activation of vascular endothelium as a determinant of its functional phenotype. *Proc Natl Acad Sci USA* 98: 4478–4485
- García-Silva S, Benito-Martín A, Nogués L, Hernández-Barranco A, Mazariegos MS, Santos V, Hergueta-Redondo M, Ximénez-Embún P, Kataru RP, Lopez AA et al (2021) Melanoma-derived small extracellular vesicles induce lymphangiogenesis and metastasis through an NGFR-dependent mechanism. *Nat Cancer* 212: 1387–1405
- Ghoroghi S, Mary B, Asokan N, Goetz JG, Hyenne V (2021a) Tumor extracellular vesicles drive metastasis (it's a long way from home). *FASEB BioAdv* 3: 930–943
- Ghoroghi S, Mary B, Larnicol A, Asokan N, Klein A, Osmani N, Busnelli I, Delalande F, Paul N, Halary S et al (2021b) Ral GTPases promote breast cancer metastasis by controlling biogenesis and organ targeting of exosomes. *Elife* 10: e61539
- Han J, Zern BJ, Shuvaev VV, Davies PF, Muro S, Muzykantov V (2012) Acute and chronic shear stress differently regulate endothelial internalization of nanocarriers targeted to platelet-endothelial cell adhesion molecule-1. *ACS Nano* 6: 8824–8836
- Han J, Shuvaev VV, Davies PF, Eckmann DM, Muro S, Muzykantov VR (2015) Flow shear stress differentially regulates endothelial uptake of nanocarriers targeted to distinct epitopes of PECAM-1. *J Control Release* 210: 39–47
- Hen G, Nicenboim J, Maysel O, Asaf L, Shin M, Busolin G, Hofi R, Almog G, Tiso N, Lawson ND et al (2015) Venous-derived angioblasts generate organ-specific vessels during zebrafish embryonic development. *Development* 142: 4266–4278
- Hoffman HK, Aguilar RS, Clark AR, Groves NS, Pezeshkian N, Bruns MM, van Engelenburg SB (2022) Endocytosed HIV-1 envelope glycoprotein traffics to Rab14 + late endosomes and lysosomes to regulate surface levels in T-cell lines. *J Virol* 96: e0076722
- Hoshino A, Costa-Silva B, Shen T-L, Rodrigues G, Hashimoto A, Tesic Mark M, Molina H, Kohsaka S, Di Giannatale A, Ceder S et al (2015) Tumour exosome integrins determine organotropic metastasis. *Nature* 527: 1–19
- Hyenne V, Apaydin A, Rodriguez D, Spiegelhalter C, Hoff-Yoessle S, Diem M, Tak S, Lefebvre O, Schwab Y, Goetz JG et al (2015) RAL-1 controls multivesicular body biogenesis and exosome secretion. *J Cell Biol* 211: 27–37
- Hyenne V, Ghoroghi S, Collot M, Bons J, Follain G, Harlepp S, Mary B, Bauer J, Mercier L, Busnelli I et al (2019) Studying the fate of tumor extracellular vesicles at high spatiotemporal resolution using the zebrafish embryo. *Dev Cell* 48: 554–572
- Imai T, Takahashi Y, Nishikawa M, Kato K, Morishita M, Yamashita T, Matsumoto A, Charoenviriyakul C, Takakura Y (2015) Macrophage-dependent clearance of systemically administered B16BL6-derived exosomes from the blood circulation in mice. *J Extracell Vesicles* 4: 26238
- Jerabkova-Roda K, Dupas A, Osmani N, Hyenne V, Goetz JG (2022) Circulating extracellular vesicles and tumor cells: sticky partners in metastasis. *Trends Cancer* 8: 799–805
- Joshi BS, de Beer MA, Giepmans BNG, Zuhorn IS (2020) Endocytosis of extracellular vesicles and release of their cargo from endosomes. *ACS Nano* 14: 4444–4455
- Kalluri R, LeBleu VS (2020) The biology, function, and biomedical applications of exosomes. *Science* 367: eaau6977

- Kienast Y, von Baumgarten L, Fuhrmann M, Klinkert WEF, Goldbrunner R, Herms J, Winkler F (2010) Real-time imaging reveals the single steps of brain metastasis formation. *Nat Med* 16: 116–122
- Kitagawa M, Hojo M, Imayoshi I, Goto M, Ando M, Ohtsuka T, Kageyama R, Miyamoto S (2013) Hes1 and Hes5 regulate vascular remodeling and arterial specification of endothelial cells in brain vascular development. *Mech Dev* 130: 458–466
- Kondapalli KC, Llongueras JP, Capilla-González V, Prasad H, Hack A, Smith C, Guerrero-Cázares H, Quiñones-Hinojosa A, Rao R (2015) A leak pathway for luminal protons in endosomes drives oncogenic signalling in glioblastoma. *Nat Commun* 6: 6289
- Kuijl C, Pilli M, Alahari SK, Janssen H, Khoo PS, Ervin KE, Calero M, Jonnalagadda S, Scheller RH, Neeffes J et al (2013) Rac and Rab GTPases dual effector Nischarin regulates vesicle maturation to facilitate survival of intracellular bacteria. *EMBO J* 32: 713–727
- Kyei GB, Vergne I, Chua J, Roberts E, Harris J, Junutula JR, Deretic V (2006) Rab14 is critical for maintenance of Mycobacterium tuberculosis phagosome maturation arrest. *EMBO J* 25: 5250–5259
- Li YS, Haga JH, Chien S (2005) Molecular basis of the effects of shear stress on vascular endothelial cells. *J Biomech* 38: 1949–1971
- Lin A, Sabnis A, Kona S, Nattama S, Patel H, Dong JF, Nguyen KT (2010) Shear-regulated uptake of nanoparticles by endothelial cells and development of endothelial-targeting nanoparticles. *J Biomed Mater Res A* 93A: 833–842
- Marar C, Starich B, Wirtz D (2021) Extracellular vesicles in immunomodulation and tumor progression. *Nat Immunol* 22: 560–570
- Mary B, Ghoroghi S, Hyenne V, Goetz JG (2020) Live tracking of extracellular vesicles in larval zebrafish. *Methods Enzymol* 645: 243–275
- Morad G, Carman CV, Hagedorn EJ, Perlin JR, Zon LI, Mustafaoglu N, Park TE, Ingber DE, Daisy CC, Moses MA (2019) Tumor-derived extracellular vesicles breach the intact blood-brain barrier via transcytosis. *ACS Nano* 13: 13853–13865
- Morioka T, Sakabe M, Ioka T, Iguchi T, Mizuta K, Hattamaru M, Sakai C, Itoh M, Sato GE, Hashimoto A et al (2014) An important role of endothelial hairy-related transcription factors in mouse vascular development. *Genesis* 52: 897–906
- Morishita M, Takahashi Y, Nishikawa M, Sano K, Kato K, Yamashita T, Imai T, Saji H, Takakura Y (2015) Quantitative analysis of tissue distribution of the B16BL6-derived exosomes using a streptavidin-lactadherin fusion protein and Iodine-125-labeled biotin derivative after intravenous injection in mice. *J Pharm Sci* 104: 705–713
- Nicoli S, Presta M (2007) The zebrafish/tumor xenograft angiogenesis assay. *Nat Protoc* 2: 2918–2923
- van Niel G, Carter DRF, Clayton A, Lambert DW, Raposo G, Vader P (2022) Challenges and directions in studying cell-cell communication by extracellular vesicles. *Nat Rev Mol Cell Biol* 23: 369–382
- Okai B, Lyall N, Gow NAR, Bain JM, Erwig LP (2015) Rab14 regulates maturation of macrophage phagosomes containing the fungal pathogen *Candida albicans* and outcome of the host-pathogen interaction. *Infect Immun* 83: 1523–1535
- Pandey E, Nour AS, Harris EN (2020) Prominent receptors of liver sinusoidal endothelial cells in liver homeostasis and disease. *Front Physiol* 11: 1–21
- Peinado H, Zhang H, Matei IR, Costa-Silva B, Hoshino A, Rodrigues G, Psaila B, Kaplan RN, Bromberg JF, Kang Y et al (2017) Pre-metastatic niches: organ-specific homes for metastases. *Nat Rev Cancer* 17: 302–317
- Perera RM, Zoncu R (2016) The lysosome as a regulatory hub. *Annu Rev Cell Dev Biol* 32: 223–253
- Qin X, Zhang K, Qiu J, Wang N, Qu K, Cui Y, Huang J, Luo L, Zhong Y, Tian T et al (2022) Uptake of oxidative stress-mediated extracellular vesicles by vascular endothelial cells under low magnitude shear stress. *Bioact Mater* 9: 397–410
- Ritchie ME, Phipson B, Wu D, Hu Y, Law CW, Shi W, Smyth GK (2015) limma powers differential expression analyses for RNA-sequencing and microarray studies. *Nucleic Acids Res* 43: e47
- Robinson MD, McCarthy DJ, Smyth GK (2009) edgeR: a Bioconductor package for differential expression analysis of digital gene expression data. *Bioinformatics* 26: 139–140
- Schindelin J, Arganda-Carreras I, Frise E, Kaynig V, Longair M, Pietzsch T, Preibisch S, Rueden C, Saalfeld S, Schmid B et al (2012) Fiji: an open-source platform for biological-image analysis. *Nat Methods* 9: 676–682
- Sheldon H, Heikamp E, Turley H, Dragovic R, Thomas P, Oon CE, Leek R, Edelmann M, Kessler B, Sainson RCA et al (2010) New mechanism for Notch signaling to endothelium at a distance by Delta-like 4 incorporation into exosomes. *Blood* 116: 2385–2394
- Shelke GV, Yin Y, Jang SC, Lässer C, Wennmalm S, Hoffmann HJ, Li L, Gho YS, Nilsson JA, Lötvall J (2019) Endosomal signalling via exosome surface TGFβ-1. *J Extracell Vesicles* 8: 1650458
- Stirling DR, Swain-Bowden MJ, Lucas AM, Carpenter AE, Cimini BA, Goodman A (2021) CellProfiler 4: improvements in speed, utility and usability. *BMC Bioinformatics* 22: 1–11
- Sung BH, von Lersner A, Guerrero J, Krystofiak ES, Inman D, Pelletier R, Zijlstra A, Ponik SM, Weaver AM (2020) A live cell reporter of exosome secretion and uptake reveals pathfinding behavior of migrating cells. *Nat Commun* 11: 1–15
- Szklarczyk D, Gable AL, Lyon D, Junge A, Wyder S, Huerta-Cepas J, Simonovic M, Doncheva NT, Morris JH, Bork P et al (2019) STRING v11: protein-protein association networks with increased coverage, supporting functional discovery in genome-wide experimental datasets. *Nucleic Acids Res* 47: D607–D613
- Takahashi Y, Nishikawa M, Shinotsuka H, Matsui Y, Ohara S, Imai T, Takakura Y (2013) Visualization and *in vivo* tracking of the exosomes of murine melanoma B16-BL6 cells in mice after intravenous injection. *J Biotechnol* 165: 77–84
- Tarbell JM (2010) Shear stress and the endothelial transport barrier. *Cardiovasc Res* 87: 320–330
- Tkach M, Théry C (2016) Communication by Extracellular Vesicles: where we are and where to go. *Cell* 164: 1226–1232
- Todorova D, Simoncini S, Lacroix R, Sabatier F, Dignat-George F (2017) Extracellular vesicles in angiogenesis. *Circ Res* 120: 1658–1673
- Trofimenko E, Homma Y, Fukuda M, Widmann C (2021) The endocytic pathway taken by cationic substances requires Rab14 but not Rab5 and Rab7. *Cell Rep* 37: 109945
- Verweij FJ, Hyenne V, Van Niel G, Goetz JG (2019a) Extracellular vesicles: catching the light in zebrafish. *Trends Cell Biol* 29: 770–776
- Verweij FJ, Revenu C, Arras G, Dingli F, Loew D, Pegtel DM, Follain G, Allio G, Goetz JG, Zimmermann P et al (2019b) Live tracking of inter-organ communication by endogenous exosomes *in vivo*. *Dev Cell* 48: 573–589
- Verweij FJ, Balaj L, Boulanger CM, Carter DRF, Compeer EB, D'Angelo G, El Andaloussi S, Goetz JG, Gross JC, Hyenne V et al (2021) The power of imaging to understand extracellular vesicle biology *in vivo*. *Nat Methods* 18: 1013–1026
- Vion AC, Kheloufi M, Hammoutene A, Poisson J, Lasselin J, Devue C, Pic I, Dupont N, Busse J, Stark K et al (2017) Autophagy is required for endothelial cell alignment and atheroprotection under physiological blood flow. *Proc Natl Acad Sci USA* 114: E8675–E8684
- Wieland E, Rodriguez-Vita J, Liebler SS, Mogler C, Moll I, Herberich SE, Espinet E, Herpel E, Menuchin A, Chang-Claude J et al (2017) Endothelial Notch1 activity facilitates metastasis. *Cancer Cell* 31: 355–367



- Xie F, Zhou X, Su P, Li H, Tu Y, Du J, Pan C, Wei X, Zheng M, Jin K et al (2022) Breast cancer cell-derived extracellular vesicles promote CD8<sup>+</sup> T cell exhaustion via TGF- $\beta$  type II receptor signaling. *Nat Commun* 13: 4461
- Yáñez-Mó M, Siljander PR-M, Andreu Z, Zavec AB, Borràs FE, Buzas EI, Buzas K, Casal E, Cappello F, Carvalho J et al (2015) Biological properties of extracellular vesicles and their physiological functions. *J Extracell Vesicles* 4: 27066



**License:** This is an open access article under the terms of the [Creative Commons Attribution-NonCommercial-NoDerivs](https://creativecommons.org/licenses/by-nc-nd/4.0/) License, which permits use and distribution in any medium, provided the original work is properly cited, the use is non-commercial and no modifications or adaptations are made.